Received May 27, 2019, accepted June 2, 2019, date of publication June 6, 2019, date of current version June 28, 2019.

Digital Object Identifier 10.1109/ACCESS.2019.2921530

Hybrid Multi-User Equalizer for Massive MIMO Millimeter-Wave Dynamic Subconnected Architecture

ROBERTO MAGUETA[1], DANIEL CASTANHEIRA[1], ADÃO SILVA[1], RUI DINIS[2], AND ATÍLIO GAMEIRO[1]

[1]Instituto de Telecomunicações (IT), and DETI, Univ.de Aveiro, 3810-193 Aveiro, Portugal
[2]Instituto de Telecomunicações (IT), and Faculdade de Ciências e Tecnologia, Univ. Nova de Lisboa, 1099-085 Lisboa, Portugal

This work was supported in part by the European Regional Development Fund (FEDER) through the Competitiveness and Internationalization Operational Program (COMPETE 2020) of the Portugal 2020 framework, Regional OP Centro (CENTRO 2020), Regional OP Lisboa (LISBOA 14-20) and by FCT/MEC through national funds, under Project MASSIVE5G (AAC n° 02/SAICT/2017) and project UID/EEA/50008/2019'', in part by the European Structural and Investment Funds through the Competitiveness and Internationalization Operational Program-COMPETE 2020, and in part by the National Funds through the Foundation for Science and Technology under the Project RETIOT under Grant POCI-01-0145-FEDER-016432.

ABSTRACT This paper proposes a hybrid multi-user equalizer for the uplink of broadband millimeter-wave massive multiple input/multiple output (MIMO) systems with dynamic subarray antennas. Hybrid subconnected architectures are more suitable for practical applications since the number of required phase shifters is lower than in fully connected architectures. We consider a set of only analog precoded users transmitting to a base station and sharing the same radio resources. At the receiver end, the hybrid multi-user equalizer is designed by minimizing the sum of the mean square error (MSE) of all subcarriers, considering a two-step approach. In the first step, the digital part is iteratively computed as a function of the analog part. It is considered that the digital equalizers are computed on a per subcarrier basis, while the analog equalizer is constant over the subcarriers and the digital iterations due to hardware constraints. In the second step, the analog equalizer with dynamic antenna mapping is derived to connect the best set of antennas to each radio frequency (RF) chain. For each subset of antennas, one antenna and a quantized phase shifter are selected at a time, taking into account all previously selected antennas. The results show that the proposed hybrid dynamic two-step equalizer achieves a performance close to the fully connected counterpart, although it is less complex in terms of hardware and signal processing requirements.

INDEX TERMS Multi-user equalizer, hybrid dynamic architecture, massive multiple input/multiple output (MIMO), millimeter-wave communications.

I. INTRODUCTION

The use of an unlicensed spectrum at a millimeter-wave (mmWave) frequency band has enabled the massive increase in wireless data associated with the next generation of wireless communications [1]. While current 4G wireless communications have bandwidths up to 20 MHz, mmWave frequencies can reach bandwidths of 2 GHz or even more [2]. However, the design of mmWave communications presents considerable challenges such as propagation difficulties (severe path loss, penetration losses and fading effects [3]). To compensate for the propagation losses, one can employ highly directional beamforming techniques using a large number of antennas [4]. In fact, the short wavelengths associated with mmWave frequencies allow packing a large antenna array in a small space, which enables the use of massive multiple input/multiple output (mMIMO) systems to form narrow beams for high beamforming gains [5]. The combination of mMIMO with mmWave is very promising, but it also presents several difficulties. For instance, the channels tend to be more correlated [6]–[8], and the power consumption and high cost of some hardware components of radio frequency (RF) chains (e.g., analog-to-digital converters (ADCs) and digital-to-analog converters (DACs), mixers, power amplifiers, etc., which can be much more complex at mmWave frequencies) make it impracticable to have one fully dedicated RF chain for each antenna; additionally, new beamforming techniques need to be developed [9], [10].

The associate editor coordinating the review of this manuscript and approving it for publication was Yunlong Cai.

To overcome these hardware limitations, a fully analog beamforming approach could be explored, using only phase shifters to reduce the complexity of implementation [11], but this limits the achievable performance and capacity since this approach is generally employed in single-stream transmissions [12]. Another option would be the use of fully digital systems with low-complexity devices (e.g., low-resolution DACs/ADCs). Although one can achieve acceptable performance at a low signal-to-noise ratio (SNR), the degradation at high SNR regions can be substantial [13].

To improve the performance of previous approaches, some hybrid architectures were proposed in [14]–[16], where part of the signal processing is implemented in the analog domain, and the remaining processing is left in the digital domain. The schemes discussed in [17]–[23], [26]–[27] and [30] considered a fully connected hybrid analog-digital architecture, since each RF chain is physically connected to all antennas. However, this architecture requires a large number of connections for a large number of antennas and/or RF chains. Therefore, schemes based on subconnected (or partially connected) hybrid architectures, where each RF chain is only connected to a subset of antennas, have been proposed. There are two main types of subconnected architectures: dynamic and fixed [30]. In the dynamic subconnected case, each RF chain can be dynamically connected to different subsets of antennas, while in the fixed subconnected case, each RF chain is always physically connected to the same subset of antennas. Precoding schemes for fixed subconnected hybrid architectures have been proposed in [24]–[27] and [29], while the dynamic case was studied in [28]–[30]. In addition to the fully connected and subconnected architectures, [31] presented one architecture where the RF chains are also divided into subsets of RF chains, and then that subset of RF chains is connected to all the antennas of the corresponding antenna subset, which is a generalization of the referred fully connected and subconnected architectures.

Since dynamic architectures are more flexible and tend to exhibit better performance, they will be considered in this paper.

A. PREVIOUS WORK ON FULLY CONNECTED ARCHITECTURES

Transmit and receive beamforming for narrowband systems were proposed for fully connected hybrid architectures in [17]–[20]. In [17], a precoder and combiner based on the spatial sparsity of the channel for the single-user multistream case were designed. For multi-user downlink systems, the authors of [18] proposed a low-complexity hybrid block diagonalization scheme. The analog precoder and combiner were designed to harvest the large array gain provided by the use of mMIMO, while the baseband processing is used to cancel the inter-user interference. A nonlinear multi-user equalizer, based on the iterative block decision feedback equalization (IB-DFE) principle [32]–[35], was proposed in [19]. In [20], a hybrid beamforming system based on a dual polarized array antenna was proposed. Two hybrid beamforming algorithms were designed using only limited feedback channel information.

Solutions for broadband systems can also be found in [21]–[23]. To solve the equalization problem in severely frequency-selective channels, hybrid precoder and codebook designs for single-user limited feedback systems were discussed in [21], where the analog precoder is constant over the subcarriers, but the digital precoder can change between subcarriers. For the multi-user case, statistical MIMO - Orthogonal Frequency Division Multiplexing (OFDM) beamformers without instantaneous channel information were designed in [22]. This was done based on analysis of the channel covariance matrices, and the beams were formed using the dominant eigenvectors to select the main directions. In [23], a hybrid precoder based on the vector quantization concept was proposed where the total transmit power is minimized.

B. PREVIOUS WORK ON SUBCONNECTED ARCHITECTURES

Schemes for fixed subconnected hybrid architectures have been proposed in [24]–[27]. In [24], a hybrid iterative block multi-user equalizer optimized using the average bit-error rate as a metric was proposed. The analog part of the equalizer was computed sequentially over the RF chains using a dictionary built from the array response vectors. A hybrid precoder was designed in [25] for multi-user systems, where the non-convex optimization problem with coupling constraints was transformed into a problem with separable constraints. Then, using block coordinate descent methods, the separable problem was solved. The authors of [26] studied a hybrid precoder structure over limited feedback channels for multi-user systems in fixed subconnected and fully connected architectures. The effect of quantized hybrid precoding was characterized, and a channel correlation-based codebook was employed, showing a clear advantage over conventional codebooks based on random vector quantization. Solutions for multi-user downlink broadband massive MIMO-OFDM systems were proposed in [27]. Hybrid beamformers were designed by maximizing the overall spectral efficiency for both hybrid fully connected and fixed subconnected architectures.

Dynamic subconnected hybrid architectures were recently addressed in [28]–[30]. He *et al.* [28] proposed a two-step algorithm for single-user narrowband systems that iteratively optimized the hybrid precoder to maximize the spectral efficiency, obtaining an extra data stream via the index of the active antenna set without any extra RF chain. A directional hybrid precoding was designed in [29] for a narrowband multi-user system with multiple eavesdroppers, considering both fixed and dynamic subconnected approaches. The goal of this design was to guarantee the receive quality of the legitimate users and to minimize the power leaked to the eavesdroppers. In [30], solutions for fully connected, fixed and dynamic subconnected OFDM hybrid precoding were designed for single-user systems, considering the sum of mutual information as an optimization metric. With this technique, the hybrid subarrays were built using long-term

characteristics of the frequency-selective mmWave channel. To our knowledge, dynamic subconnected hybrid techniques for the uplink of multi-user broadband mmWave massive MIMO systems have yet to be addressed in the literature.

C. MAIN CONTRIBUTIONS

In this paper, we propose a solution for the uplink of multi-user broadband mmWave mMIMO systems that addresses the complexity and power consumption issues of these systems. Therefore, our design options include the following:

- The use of SC-FDMA, which can cope with multi-path effects as well as the popular OFDM schemes, but the transmitted signals have a much lower peak-to-average power ratio (PAPR).
- To keep the user terminals (UTs) simple, reduce the hardware costs and power consumption, an analog-only precoder is considered for the UTs. The analog precoder does not require full channel state information (CSI) knowledge, and the CSI estimation complexity is shifted to the base station (BS).
- The use of a dynamic subconnected hybrid architecture at the BS requires fewer phase shifters and physical connections between the antennas and RF chains than the fully connected counterpart.

It is well known that linear multi-user equalizers are not the best ones for SC-FDMA systems due to the residual interference. It has been shown that nonlinear/iterative multi-user equalizers, in particular the ones based the IB-DFE principle, outperforms linear ones and have excellent performance–complexity tradeoffs [37]. Considering hybrid architectures, the design of joint iterative/nonlinear analog and digital equalizer is not practical, since it would require the storage of analog signals to apply the iterative structure in the analog domain. Therefore, we design a sub-optimal two-step approach. In the first step, the closed-form iterative digital equalizer is obtained as a function of the analog part of the equalizer. In the second one, the analog equalizer with dynamic antenna mapping, is derived assuming that the digital part will fully remove the interference. The main contributions of this paper are as follows:

- Design a new hybrid dynamic subconnected two-step multi-user equalizer based on minimization of the sum of the mean square error (MSE) of all subcarriers, which is shown to be equivalent to minimizing the weighted error between the hybrid dynamic equalizer and the fully digital one.
  - The digital part is computed iteratively over the subcarriers based on the IB-DFE principle. The feedforward and feedback matrices are obtained as functions of the analog part.
  - Design an analog equalizer with a dynamic antenna architecture. The algorithm selects the best antenna mapping and the corresponding quantized phase shifter for each radio frequency (RF) chain. This is done sequentially by considering the previous antenna map and phase shifter values to select a new antenna and phase shifter.

TABLE 1. Notations adopted in the paper.

Operator	Description
$\mathrm{tr}(.)$	Trace of a matrix.
$(.)^{*}$	Conjugate of a matrix.
$(.)^{T}$	Transpose of a matrix.
$(.)^{H}$	Hermitian of a matrix.
$\{\alpha_k\}_{k=1}^{S}$	Represents the S -length block.
$\mathrm{diag}(\mathbf{a})$	Diagonal matrix where the diagonal entries are equal to vector $\mathbf{a}$.
$\mathrm{diag}(\mathbf{A})$	Vector equal the diagonal entries of the matrix $\mathbf{A}$.
$\mathbf{A}(n,m)$	Represents the element of the nth row and mth column of $\mathbf{A}$.
$\mathbf{I}_N$	Identity matrix $N \times N$.
$\mathbf{e}_u$	$\mathbf{e}_u \in \mathbb{C}^U$ is a U -length vector of zeros with the uth entry equal to one.
$\Omega \setminus \Lambda$	Set of values from Ω , except the set of values from Λ .
t, k and u	Represent the time, subcarrier and user terminal indexes, respectively.

- Proposal a simple yet accurate semianalytical approach for obtaining the performance of the proposed hybrid dynamic receiver structure.
- Analysis of the computational complexity of the proposed algorithm.

The numerical results show that the proposed dynamic subconnected hybrid multi-user equalizer outperforms the fixed subconnected counterpart and almost achieves the performance of the fully connected one.

The remainder of this paper is structured as follows: Section II describes the system model adopted in the paper. In Section III, we design the hybrid dynamic subconnected iterative analog-digital multi-user equalizer. In Section IV, we show the main performance results. Finally, the main conclusions of the paper are presented in Section V.

D. NOTATIONS

Capital boldface letters denote matrices, and lower boldface letters denote column vectors. The remaining notations in this paper are presented in Table 1.

II. SYSTEM MODEL CHARACTERIZATION

In this paper, we consider an uplink broadband mmWave system with N_c available subcarriers and using SC-FDMA as the access technique. We assume that the system has U UTs sharing the same radio resources and one BS.

A. USER TERMINAL DESCRIPTION

Each UT transmits a single data stream per subcarrier and has N_{tx} antennas. The block diagram of the uth UT is shown in Fig. 1. We consider M-QAM constellations, where $s_{u,t}$, $t \in \{1, \ldots, N_c\}$ denotes a data symbol with $\mathbb{E}[|s_{u,t}|^2] = \sigma_u^2$.

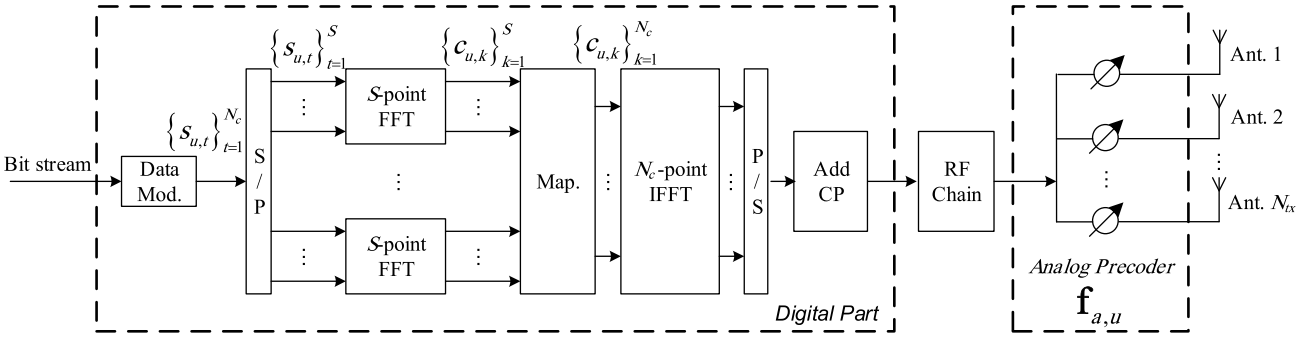

FIGURE 1. Block diagram of the uth UT.

We also consider G data blocks with $S = N_c/G$ length, where $\{s_{u,t}\}_{t=(g-1)S+1}^{gS}$ is the gth data block of sequence $\{s_{u,t}\}_{t=1}^{N_c}$. Moreover, the DFT of $\{s_{u,t}\}_{t=(g-1)S+1}^{gS}$ is denoted as $\{c_{u,k}\}_{k=(g-1)S+1}^{gS}$. For the sake of simplicity, the index g is omitted once each S-length data block is processed independently. Therefore, hereinafter, the block is denoted as $\{s_{u,t}\}_{t=1}^{S}$, and its DFT is denoted as $\{c_{u,k}\}_{k=1}^{S}$. After the DFT, the data in the frequency domain are interleaved to increase the diversity order and mapped in the OFDM symbol. To end, the cyclic prefix (CP) is added. The analog precoder employed at the UT is mathematically modeled by $\mathbf{f}_{a,u} \in \mathbb{C}^{N_{tx}}$. This represents the physical analog phase shifters, which require that all elements of $\mathbf{f}_{a,u}$ must have an equal magnitude, i.e., $|\mathbf{f}_{a,u}(n)|^2 = N_{tx}^{-1}$.

For the uth user at the kth subcarrier, the discrete transmit baseband signal $\mathbf{x}_{u,k} \in \mathbb{C}^{N_{tx}}$ may be mathematically described by

$$\mathbf{x}_{u,k} = \mathbf{f}_{a,u} c_{u,k}, \tag{1}$$

where $c_{u,k} \in \mathbb{C}$. The analog precoder $\mathbf{f}_{a,u}$ does not have a subcarrier index k, since an analog precoder computed on a per subcarrier basis would require SN_{tx} phase shifters, which can be impractical. For complexity reasons, a decoupled transmitter-receiver optimization problem is also assumed, and since the aim of this paper is to design a hybrid multi-user equalizer, we consider a low-complexity analog precoder based on the average angles of arrival (AoD) discussed in [40].

B. BASE STATION DESCRIPTION

The BS has N_{rx} antennas and N_{rx}^{RF} RF chains. A hybrid analog-digital architecture with a dynamic subarray structure is considered for the BS. In the analog part, each RF chain is only connected to a subset of $R = N_{rx}/N_{rx}^{RF}$ antennas chosen dynamically. The fully connected, fixed sub-connected and dynamic sub-connected architectures are represented in Fig. 2 a), b) and c), respectively. The considered system has the parameter constraint $U \leq N_{rx}^{RF} \leq N_{rx}$.

The received signal $\mathbf{y}_k$ at the kth subcarrier is given by

$$\mathbf{y}_k = \sum_{u=1}^{U} \mathbf{H}_{u,k}\mathbf{x}_{u,k} + \mathbf{n}_k \ , \tag{2}$$

where $\mathbf{H}_{u,k} \in \mathbb{C}^{N_{rx}\times N_{tx}}$ denote the channel of the uth UT and $\mathbf{n}_k \in \mathbb{C}^{N_{rx}}$ the zero-mean Gaussian noise with σ_n^2 variance.

To recover the transmitted data from the received signal a hybrid multi-user equalizer with a digital iterative procedure is considered at the receiver. As shown in Fig. 3, the received signal is firstly processed by the analog part of the equalizer through the analog phase shifters. Then, the signal is processed by the N_{rx}^{RF} RF chains and goes through digital iterative processing composed of a closed loop with forward and feedback paths. Therefore, the received signal at the kth subcarrier and ith iteration is given by

$$\tilde{\mathbf{c}}_k^{(i)} = \mathbf{W}_{d,k}^{(i)}(\mathbf{W}_a)^H\mathbf{y}_k - \mathbf{B}_{d,k}^{(i)}\hat{\mathbf{c}}_k^{(i-1)}, \tag{3}$$

where $\tilde{\mathbf{c}}_k^{(i)} = [\,\tilde{c}_{1,k}^{(i)} \cdots \tilde{c}_{U,k}^{(i)}\,]^T \in \mathbb{C}^U$ is the concatenation of the processed received signal of all UTs. The matrix $\mathbf{W}_a \in \mathbb{C}^{N_{rx}\times N_{rx}^{RF}}$ represents the analog equalizer fixed over the subcarriers, and the matrices $\mathbf{W}_{d,k}^{(i)} \in \mathbb{C}^{U\times N_{rx}^{RF}}$ and $\mathbf{B}_{d,k}^{(i)} \in \mathbb{C}^{U\times U}$ are the digital feedforward and digital feedback coefficients at the ith iteration and the kth subcarrier, respectively. The magnitude of the analog equalizer coefficients is restricted to be either 0 or $R^{-1/2}$, i.e., $|\mathbf{W}_a(n,l)|^2 \in \{0, R^{-1}\}$, $\forall n \in \{1,\ldots,N_{rx}\}$, $l \in \{1,\ldots,N_{rx}^{RF}\}$. For the uth UT at the ith iteration, we have $\hat{\mathbf{c}}_k^{(i)} = \left[\,\hat{c}_{1,k}^{(i)} \cdots \hat{c}_{U,k}^{(i)}\,\right]^T \in \mathbb{C}^U$, where the sequence $\left\{\hat{c}_{u,k}^{(i)}\right\}_{k=1}^{S}$ is the FFT of $\left\{\hat{s}_{u,t}^{(i)}\right\}_{t=1}^{S}$, i.e., the FFT of time domain data estimates. Moreover, the symbols $\hat{s}_{u,t}^{(i)}$ represent the hard decisions associated with the M-QAM constellation.

C. CHANNEL MODEL

A clustered channel model with N_{cl} clusters and N_{ray} propagation paths per cluster was adopted. For the uth UT, the delay-d channel matrix $\mathbf{H}_{u,d} \in \mathbb{C}^{N_{rx}\times N_{tx}}$, such that $\mathbb{E}[\|\mathbf{H}_{u,d}\|_F^2] = N_{rx}N_{tx}$, may be expressed as

$$\mathbf{H}_{u,d} = \sqrt{\frac{N_{rx}N_{tx}}{\rho_{PL}}} \sum_{q=1}^{N_{cl}}\sum_{l=1}^{N_{ray}} \Big(\alpha_{q,l}^u p_{rc}(dT_s - \tau_q^u - \tau_{q,l}^u) \times \mathbf{a}_{tx,u}(\theta_q^u - \vartheta_{q,l}^u)\mathbf{a}_{rx,u}^H(\phi_q^u - \varphi_{q,l}^u)\Big), \tag{4}$$

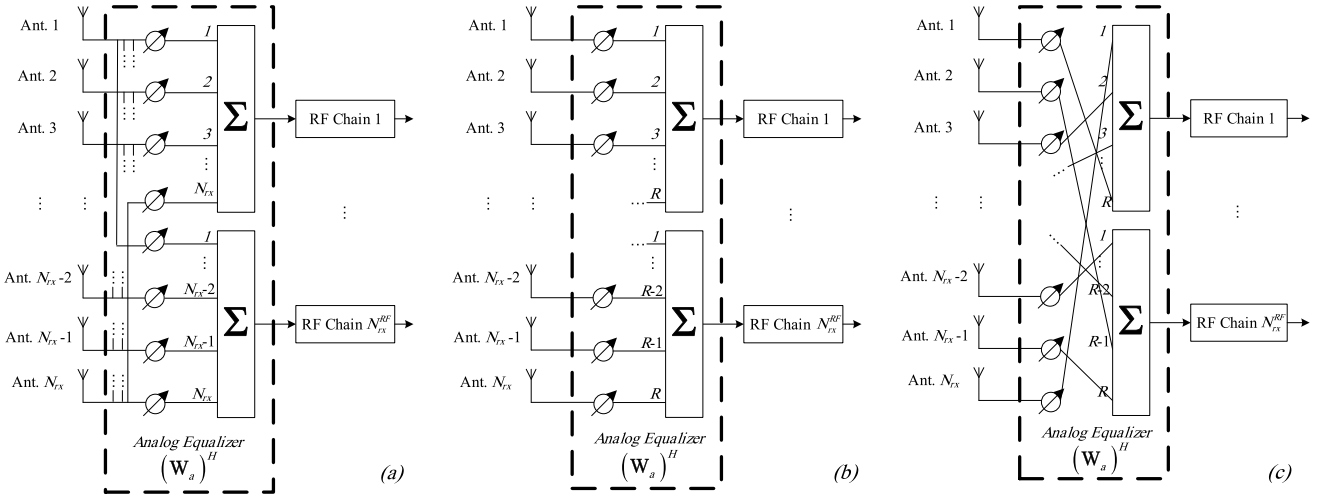

FIGURE 2. Analog part: (a) fully connected; (b) subconnected with fixed subarray; (c) subconnected with dynamic subarray.

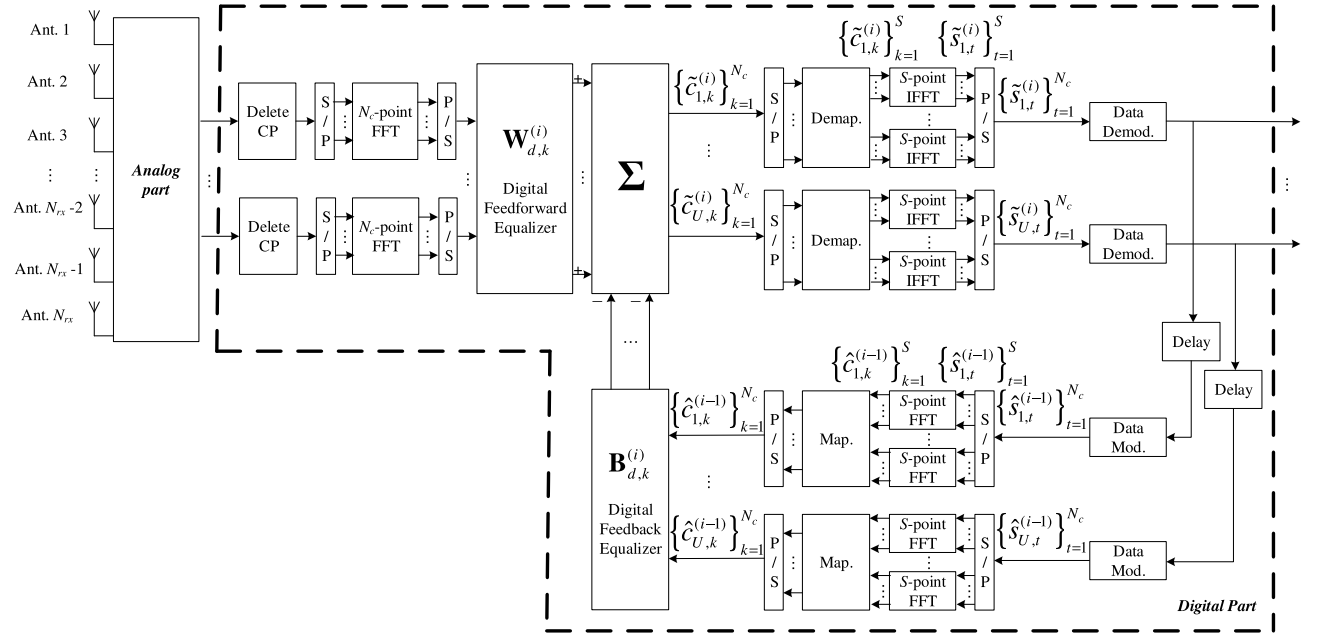

FIGURE 3. Proposed receiver structure.

and its frequency domain version at subcarrier k as

$$\mathbf{H}_{u,k} = \sum_{d=0}^{D-1} \mathbf{H}_{u,d} e^{-j\frac{2\pi k}{N_c}d}. \tag{5}$$

The path delays are uniformly distributed in $[0, DT_s]$, where T_S is the sampling interval and D is the cyclic prefix length. The path loss between the UT and the BS is ρ_{PL}, while the lth ray in the qth cluster has a complex path gain equal to $\alpha_{q,l}^u$. The function $p_{rc}(.)$ is a rectangular window. The angles of arrival ϕ_q^u (AoA) and departure θ_q^u(AoD) of qth cluster, and the relative angles of arrival $\varphi_{q,l}^u$ and departure $\vartheta_{q,l}^u$ of the lth ray from qth cluster, have the random distribution presented in [21]. The qth cluster has a time delay τ_q^u, and its lth ray has a relative time delay equal to$\tau_{q,l}^u$. The vectors $\mathbf{a}_{rx,u}$ and $\mathbf{a}_{tx,u}$ are the normalized receive and transmit array response vectors of uth UT, respectively, given for an N-element uniform linear array (ULA) by

$$\mathbf{a}_{ULA}(\theta) = \frac{1}{\sqrt{N}}\left[1, e^{j2\pi\frac{\gamma}{\lambda}\sin(\theta)}, \ldots, e^{j2\pi\frac{\gamma}{\lambda}\sin(\theta)(N-1)}\right]^T, \tag{6}$$

where λ and γ are the wavelength and the interelement spacing, respectively. The channel matrix of the uth UT at the kth subcarrier can also be written as

$$\mathbf{H}_{u,k} = \mathbf{A}_{rx,u}\mathbf{\Delta}_{u,k}\mathbf{A}_{tx,u}^H, \tag{7}$$

where the paths gain of the lth ray from the qth cluster comprise the diagonal of diagonal matrix $\mathbf{\Delta}_{u,k} \in \mathbb{C}^{N_{cl}N_{ray}\times N_{cl}N_{ray}}$. $\mathbf{A}_{tx,u} = [\mathbf{a}_{tx,u}(\theta_1^u - \vartheta_{1,1}^u), \ldots, \mathbf{a}_{tx,u}(\theta_{N_{cl}}^u - \vartheta_{N_{cl},N_{ray}}^u))] \in \mathbb{C}^{N_{tx}\times N_{cl}N_{ray}}$ and $\mathbf{A}_{rx,u} = [\mathbf{a}_{rx,u}(\phi_1^u - \varphi_{1,1}^u), \ldots, \mathbf{a}_{rx,u}(\phi_{N_{cl}}^u - \varphi_{N_{cl},N_{ray}}^u))] \in \mathbb{C}^{N_{rx}\times N_{cl}N_{ray}}$ are the matrices of the uth user

corresponding to the concatenation of all transmit and receive array response vectors, respectively.

III. HYBRID MULTI-USER EQUALIZER DESIGN

The design of joint iterative analog and digital equalizers is not feasible, since it would require the storage of analog signals to apply the iterative structure in the analog domain. Therefore, a sub-optimal two-step hybrid multi-user receiver structure with a dynamic subarray is designed in this section. The main challenge relative to the fixed subconnected subarray architecture is the necessity to design an efficient algorithm to dynamically map the antennas to the RF chains. In the following derivation, the closed-form iterative digital equalizer is firstly obtained as a function of the analog part of the equalizer. Then, the analog equalizer with dynamic antenna mapping, which cannot be obtained iteratively, is derived assuming that the digital part will fully remove the interference. Finally, the digital equalizer is iteratively computed using the analog fixed coefficients.

A. DIGITAL PART OF EQUALIZER

In this section, we describe in detail the digital part of the equalizer. In [40] and [41], a brief discussion was provided for fixed fully connected and subconnected architectures, respectively. As previously mentioned, the hybrid equalizer is designed by minimizing the sum of the MSE of all subcarriers. Mathematically, the optimization problem may be formulated as

$$\begin{aligned}\left(\mathbf{W}_a, \mathbf{W}_{d,k}^{(i)}, \mathbf{B}_{d,k}^{(i)}\right) &= \arg\min \sum_{k=1}^{S} \mathrm{MSE}_k^{(i)} \\ &\text{s.t.} \sum_{k=1}^{S} \mathrm{diag}(\mathbf{W}_{d,k}^{(i)}(\mathbf{W}_a)^H \mathbf{H}_k) = S\mathbf{I}_U \\ &\mathbf{W}_a \in \mathcal{W}_a\ , \end{aligned} \tag{8}$$

where $\mathbf{H}_k = \left[\mathbf{H}_{1,k}\mathbf{f}_{a,1} \cdots \mathbf{H}_{U,k}\mathbf{f}_{a,U}\right] \in \mathbb{C}^{N_{rx}\times U}$ is the overall equivalent channel at the kth subcarrier and $\mathcal{W}_a$ denotes the set of feasible analog coefficients. The power constraint of (8) is imposed to avoid biased estimates [36]. The MSE at the ith iteration and kth subcarrier, $\mathrm{MSE}_k^{(i)}$, derived in Appendix A, is given by

$$\begin{aligned}\mathrm{MSE}_k^{(i)} &= \mathbb{E}[||\tilde{\mathbf{c}}_k^{(i)} - \mathbf{c}_k||^2] \\ &= \left\|\mathbf{W}_{ad,k}^{(i)}\mathbf{H}_k - \mathbf{B}_{d,k}^{(i)}\Psi^{(i-1)} - \mathbf{I}_U\right\|_F^2 \sigma_u^2 \\ &\quad + \left\|\mathbf{B}_{d,k}^{(i)}(\mathbf{I}_U - |\Psi^{(i-1)}|^2)^{1/2}\right\|_F^2 \sigma_u^2 \\ &\quad + \left\|\mathbf{W}_{ad,k}^{(i)}\right\|_F^2 \sigma_n^2\ , \end{aligned} \tag{9}$$

where $\mathbf{W}_{ad,k}^{(i)} = \mathbf{W}_{d,k}^{(i)}(\mathbf{W}_a)^H$. $\Psi^{(i)} \in \mathbb{C}^{U\times U}$ is a blockwise reliability measure matrix, which is diagonal and whose uth diagonal element gives the measure associated with uth block at the ith iteration [32]. The correlation coefficients of $\Psi^{(i)}$ for QPSK and for high-order modulations can be estimated at the BS, as presented in [36] and [34], respectively.

For an M-QAM constellation with Gray mapping, the average BER is given by

$$\mathrm{BER} = \frac{\alpha}{US}\sum_{u=1}^{U}\sum_{k=1}^{S} Q\left(\sqrt{\beta\left(\mathrm{MSE}_{k,u}^{(i)}\right)^{-1}}\right), \tag{10}$$

where $\alpha = 4(1 - 1/\sqrt{M})/\log_2[M]$, $\beta = 3/(M-1)$, $Q(.)$ denotes the Q-function, $\mathrm{MSE}_{k,u}^{(i)}$ is the mean square error on samples $\tilde{c}_{k,u}^{(i)}$, with $\mathrm{MSE}_k^{(i)} = \sum_{u=1}^{U}\mathrm{MSE}_{k,u}^{(i)}$, at iteration i.

To find the feedback matrix $\mathbf{B}_{d,k}^{(i)}$, we can consider the unconstrained optimization problem (8) once $\mathbf{B}_{d,k}^{(i)}$ is independent of the problem constraints, i.e.,

$$\mathbf{B}_{d,k}^{(i)} = \arg\min \sum_{k=1}^{S} \mathrm{MSE}_k^{(i)}\ , \tag{11}$$

whose solution is obtained from the KKT conditions, $\partial\left(\sum_{k=1}^{S}\mathrm{MSE}_k^{(i)}\right)\Big/\partial\left(\mathbf{B}_{d,k}^{(i)}\right) = \mathbf{0}$, and given by

$$\mathbf{B}_{d,k}^{(i)} = \left(\mathbf{W}_{d,k}^{(i)}(\mathbf{W}_a)^H\mathbf{H}_k - \mathbf{I}_U\right)\left(\Psi^{(i-1)}\right)^H\ . \tag{12}$$

By replacing (12) in (9), we have $\mathrm{MSE}_k^{(i)} = \sigma_u^2\overline{\mathrm{MSE}}_k^{(i)} + c$, where c is a constant independent of the optimization problem variables, as shown in Appendix B, with

$$\overline{\mathrm{MSE}}_k^{(i)} = \left\|\left(\mathbf{W}_{d,k}^{(i)}(\mathbf{W}_a)^H - \overline{\mathbf{W}}_{fd,k}^{(i)}\right)\left(\tilde{\mathbf{R}}_k^{(i-1)}\right)^{1/2}\right\|_F^2, \tag{13}$$

$$\overline{\mathbf{W}}_{fd,k}^{(i)} = (\mathbf{I}_U - |\Psi^{(i-1)}|^2)\mathbf{H}_k^H\left(\tilde{\mathbf{R}}_k^{(i-1)}\right)^{-1}\ , \tag{14}$$

$$\tilde{\mathbf{R}}_k^{(i-1)} = \mathbf{H}_k(\mathbf{I}_U - |\Psi^{(i-1)}|^2)\mathbf{H}_k^H + \sigma_n^2\sigma_u^{-2}\mathbf{I}_{N_{rx}}. \tag{15}$$

The matrix $\overline{\mathbf{W}}_{fd,k}^{(i)}$ denotes the non-normalized fully digital equalizer, derived in Appendix C. Note that the use of $\mathrm{MSE}_k^{(i)}$ or $\overline{\mathrm{MSE}}_k^{(i)}$ in the objective function of problem (8) does not affect its solution since $\mathrm{MSE}_k^{(i)}$ is equal to $\overline{\mathrm{MSE}}_k^{(i)}$ up to a constant. This means that the minimization of the $\mathrm{MSE}_k^{(i)}$ given by (9) is equivalent to the minimization of the weighted error between the hybrid equalizer and the non-normalized fully digital, $\overline{\mathrm{MSE}}_k^{(i)}$, given by (13). Therefore, the digital feedforward equalizer $\mathbf{W}_{d,k}^{(i)}$, as a function of the analog equalizer $\mathbf{W}_a$, is obtained from the optimization problem,

$$\begin{aligned}\mathbf{W}_{d,k}^{(i)}[\mathbf{W}_a] &= \arg\min \sum_{k=1}^{S} \overline{\mathrm{MSE}}_k^{(i)} \\ &\text{s.t.} \sum_{k=1}^{S} \mathrm{diag}(\mathbf{W}_{d,k}^{(i)}(\mathbf{W}_a)^H\mathbf{H}_k) = S\mathbf{I}_U, \end{aligned} \tag{16}$$

and it has the following solution as demonstrated in Appendix D,

$$\mathbf{W}_{d,k}^{(i)}[\mathbf{W}_a] = \Omega_d\mathbf{H}_k^H\mathbf{W}_a\left(\mathbf{R}_{d,k}^{(i-1)}\right)^{-1}\ , \tag{17}$$

where

$$\Omega_d = S\left(\sum_{k=1}^{S}\text{diag}\left(\mathbf{H}_k^H\mathbf{W}_a\left(\mathbf{R}_{d,k}^{(i-1)}\right)^{-1}(\mathbf{W}_a)^H\mathbf{H}_k\right)\right)^{-1}, \quad (18)$$

$$\mathbf{R}_{d,k}^{(i-1)} = (\mathbf{W}_a)^H\tilde{\mathbf{R}}_k^{(i-1)}\mathbf{W}_a. \quad (19)$$

The matrix Ω_d forces the power constraint of (16). The solution (17) is a stationary point of the optimization problem (16), since the partial derivatives of the associated Lagrangian vanish at this point, as shown in Appendix D.

The pseudocode used to compute the digital part of the equalizer as a function of the analog equalizer is presented in Algorithm 1. Initially, $\Psi^{(0)} = \mathbf{0}_U$ and the iterative digital equalizer reduces to the standard minimum mean square error (MMSE) equalizer. For each iteration $i > 0$, a new blockwise reliability measure matrix $\Psi^{(i)}$ is computed and the feedforward and feedback equalizer matrices $\mathbf{W}_{d,k}^{(i)}$ and $\mathbf{B}_{d,k}^{(i)}$, respectively, are updated.

B. ANALOG EQUALIZER WITH DYNAMIC ANTENNA MAPPING DESIGN

As mentioned, the analog equalizer should remain constant over the digital iterations due to hardware constraints. Therefore, to calculate the result, we need to fix the coefficients of matrix $\mathbf{\Psi}^{(i)}$ computed in the iterative digital part. This matrix represents a crucial parameter to ensure good receiver performance because it supplies a blockwise reliability measure of the estimates employed in the feedback loop [19], [40]. As the number of iterations increases, the estimates are more reliable, and the coefficients tend toward 1. Therefore, to compute the analog phase shifters, we consider this extreme case, where the estimates are fully reliable, and from (14), $\overline{\mathbf{W}}_{fd,k}^{(i)}$ is equivalent to the maximal ratio combining (MRC) equalizer

$$\overline{\mathbf{W}}_{fd,k} = \mathbf{H}_k^H. \quad (20)$$

From the definition of $\overline{\mathbf{W}}_{fd,k}^{(i)}$ given by (14), the $\tilde{\mathbf{R}}_k$ matrix is

$$\tilde{\mathbf{R}}_k = \sigma_n^2\sigma_u^{-2}\mathbf{I}_U \ . \quad (21)$$

To optimize the analog part of the hybrid equalizer, we consider a sequential procedure over the RF chains and antennas; i.e., for each RF chain, a set of antennas connected to it is dynamically selected.

Let $\mathbf{w}_{a,r} \in \mathbb{C}^{N_{rx}}$ be the equalizer vector of the rth RF chain (which corresponds to the rth column of $\mathbf{W}_a$) and define $\mathbf{W}_{ad,k,r} = \mathbf{W}_{d,k,r}(\mathbf{W}_{a,r})^H$, which corresponds to feedforward analog-digital equalizer, with $\mathbf{W}_{a,r} = [\mathbf{w}_{a,1}, \ldots, \mathbf{w}_{a,r}] \in \mathbb{C}^{N_{rx}\times r}$ and $\mathbf{W}_{d,k,r} = [\mathbf{w}_{d,k,1}, \ldots, \mathbf{w}_{d,k,r}] \in \mathbb{C}^{U\times r}$, where $\mathbf{w}_{d,k,r} \in \mathbb{C}^U$. As $\mathbf{W}_{d,k,r} = [\mathbf{W}_{d,k,r-1}, \mathbf{w}_{d,k,r}]$ and $\mathbf{W}_{a,r} = [\mathbf{W}_{a,r-1}, \mathbf{w}_{a,r}]$, the hybrid equalizer at the rth step can be given by

$$\mathbf{W}_{ad,k,r} = \mathbf{W}_{ad,k,r-1} + \mathbf{w}_{d,k,r}\left(\mathbf{w}_{a,r}\right)^H \ , \quad (22)$$

for $r = 1, \ldots, N_{rx}^{RF}$. At the rth step of the algorithm, $\mathbf{W}_{ad,k,r-1}$ is already known because the matrix $\mathbf{W}_{a,r-1}$ was computed in the previous steps, and $\mathbf{W}_{d,k,r-1}$ can be computed by (17) for $\Psi = \mathbf{I}_U$. Replacing (22) in (13), we obtain the optimization problem that allows for finding the analog vector that satisfies (8).

$$\mathbf{w}_{a,r} = \arg\min \sum_{k=1}^{S}\left\|\mathbf{w}_{d,k,r}\mathbf{w}_{a,r}^H - \mathbf{W}_{res,k,r-1}\right\|_F^2 \quad \text{s.t. } \mathbf{w}_{a,r} \in \mathcal{F}_{a,r}\ , \quad (23)$$

where $\mathcal{F}_{a,r}$, for step r, denotes the set of feasible analog vectors. The difference between the nonnormalized fully digital equalizer and the hybrid equalizer is denoted here as a residue matrix, given by $\mathbf{W}_{res,k,r-1} = \overline{\mathbf{W}}_{fd,k} - \mathbf{W}_{ad,k,r-1}$. The receive amplitude constraint of (8) does not appear in (23) because it is assured by (17) in the digital feedforward equalizer equation.

It can be shown that from the KKT conditions of (23), the rth vector of digital feedforward equalizer is

$$\mathbf{w}_{d,k,r} = \mathbf{W}_{res,k,r-1}\mathbf{w}_{a,r}\left(\mathbf{w}_{a,r}^H\mathbf{w}_{a,r}\right)^{-1}. \quad (24)$$

Replacing (24) in (23), the objective function of (23) is equivalent to

$$\begin{aligned}&\sum_{k=1}^{S}\left\|\mathbf{w}_{d,k,r}\mathbf{w}_{a,r}^H - \mathbf{W}_{res,k,r-1}\right\|_F^2\\ &= \sum_{k=1}^{S}\text{tr}\left\{\mathbf{W}_{res,k,r-1}\mathbf{W}_{res,k,r-1}^H\right\}\\ &\quad -\sum_{k=1}^{S}\text{tr}\left\{\mathbf{W}_{res,k,r-1}\mathbf{w}_{a,r}\left(\mathbf{w}_{a,r}^H\mathbf{w}_{a,r}\right)^{-1}\mathbf{w}_{a,r}^H\mathbf{W}_{res,k,r-1}^H\right\}, \quad (25)\end{aligned}$$

where we can see that the first term of (25) is independent of $\mathbf{w}_{a,r}$, while the second term is a correlation involving $\mathbf{w}_{a,r}$. Thus, by maximizing the second term of (25), we minimize the objective function of (23), i.e., solving the referred optimization problem. Then, we use this term as a metric to select the best vector from $\mathcal{F}_{a,r}$ to build the analog equalizer. This term is equivalent to

$$\sum_{k=1}^{S}\frac{\mathbf{w}_{a,r}^H\mathbf{W}_{res,k,r-1}^H\mathbf{W}_{res,k,r-1}\mathbf{w}_{a,r}}{\mathbf{w}_{a,r}^H\mathbf{w}_{a,r}} = \sum_{k=1}^{S}\frac{\left\|\mathbf{W}_{res,k,r-1}\mathbf{w}_{a,r}\right\|^2}{\left\|\mathbf{w}_{a,r}\right\|^2}. \quad (26)$$

Therefore, the new optimization problem (23) can be simplified to

$$\mathbf{w}_{a,r} = \arg\max \sum_{k=1}^{S}\frac{\left\|\mathbf{W}_{res,k,r-1}\mathbf{w}_{a,r}\right\|^2}{\left\|\mathbf{w}_{a,r}\right\|^2} \quad \text{s.t. } \mathbf{w}_{a,r} \in \mathcal{F}_{a,r}\ . \quad (27)$$

As previously mentioned for the dynamic subarray structure each RF chain is only connected to a subset of R antennas. Therefore, the codebook to compute (27) is defined as the set of vectors with R nonzero entries, which results in a codebook with a cardinality ${}^{N_{rx}}C_R$. For practical values of N_{rx} and R, this results in a very large codebook dimension. Therefore,

to simplify the search process, the procedure is divided into R steps, where in each step, one antenna is selected. The antennas selected in previous steps are not considered in the next steps. Please note that R steps are required per RF chain. In the following the steps are indexed by variable $m \in \{1, \ldots, R\}$. Let $\mathcal{A} = \{1, \ldots, N_{rx}\}$ denote the set of all antenna indexes, $\mathcal{I}_r$, $r \in \{1, \ldots, N_{rx}^{RF}\}$ the set of all indexes of the previously selected antennas of the rth RF chain and define $\mathcal{I} = \mathcal{I}_1 \cup \ldots \cup \mathcal{I}_r$ as the set of all selected antenna indexes up to the rth RF chain, then $\mathbf{w}_{a,r} \in \mathbb{C}^{N_{rx}}$ may be decomposed as

$$\mathbf{w}_{a,r} = \mathbf{w}_{a,r}(p)\mathbf{e}_p + \mathbf{w}_{\mathcal{I}_r} + \sum_{b \in \mathcal{A}\backslash\{\mathcal{I}\cup p\}} \mathbf{w}_{a,r}(b)\mathbf{e}_b \quad (28)$$

where $\mathbf{w}_{\mathcal{I}_r} = \sum_{q\in\mathcal{I}_r} \mathbf{w}_{a,r}(q)\mathbf{e}_q$ and $p \in \mathcal{A}\backslash\mathcal{I}$ denotes the index of the antenna to be connected to the rth RF chain in the current step. Since only one antenna is connected per step $\mathbf{w}_{a,r}(b) = 0, \forall b \in \mathcal{A}\backslash\{\mathcal{I} \cup p\}$. Therefore, the objective of the step m is to select index p from the set $\mathcal{A}\backslash\mathcal{I}$ and the value of the corresponding rth RF chain phase shifter ($\mathbf{w}_{a,r}(p)$) from the set of complex numbers with magnitude R^{-1}, denoted by $\mathcal{M}$ in the following. Let $\mathcal{M}_d = \left\{R^{-1/2}e^{j2\pi\Delta/N_\Delta},\ \Delta = 0, \ldots, N_\Delta - 1\right\}$, denote the discrete version of set $\mathcal{M}$ with $N_\Delta = 2^b$, where b is the number of quantization bits, then entry p of $\mathbf{w}_{a,r}$ may be parametrized as $\mathbf{w}_{a,r}(p) = R^{-1/2}e^{j2\pi\Delta/N_\Delta}$, with $\Delta \in \{0, \ldots, N_\Delta - 1\}$. From the previous statements and accordingly to (28) the optimization problem (27) at step the m simplifies to

$$\begin{aligned} \mathbf{w}_{a,r}(p) = \arg \max_{(\mathbf{w}_{a,r}(p),p)} & \ \mathrm{f}(p, \mathbf{w}_{a,r}(p)) \\ \text{s.t. } & p \in \mathcal{A}\backslash\mathcal{I}, \\ & \mathbf{w}_{a,r}(p) = R^{-1/2}e^{j2\pi\Delta/N_\Delta}, \\ & \Delta \in \{0, \ldots, N_\Delta - 1\}, \end{aligned} \quad (29)$$

where

$$\mathrm{f}(p, x) = \sum_{k=1}^{S} \frac{\left\|\mathbf{W}_{res,k,r-1}\left(x\mathbf{e}_p + \mathbf{w}_{\mathcal{I}_r}\right)\right\|^2}{\left\|x\mathbf{e}_p + \mathbf{w}_{\mathcal{I}_r}\right\|^2}. \quad (30)$$

Please note that problem (29) may be solved by considering all pairs from the set $\mathcal{S} = \{(p, \Delta)|p \in \mathcal{A}\backslash\mathcal{I}, \Delta \in \{0, \ldots, N_\Delta - 1\}\}$ and selecting the one which maximizes $\mathrm{f}\left(p, R^{-1/2}e^{j2\pi\Delta/N_\Delta}\right)$. It should be pointed out that since the full space of solutions is considered, when optimizing (29), the obtained solution is optimal. However, as a sequential approach is used to obtain the analog equalizer matrix, the obtained solution may not correspond to the global optimum point of problem (8), which is a combinatorial optimization problem.

The pseudocode of this optimization problem is presented in Algorithm 2. For the rth RF chain, we need to select R antennas from the available $N_{rx} - R(r-1)$ antennas, with $\mathbf{W}_{res,k,r-1}$ and $\mathcal{I}$ as inputs that represent the residue and the set of selected antenna indexes until the rth RF chain. From rows 2 to 5, the metric of (29) is computed for all phases and remaining antennas. Then, the best antenna and phase indexes are selected in row 6. From this information, the analog equalizer is computed for the rth RF chain. After that, the antenna indexes are updated to select the next antenna of this RF chain. Finally, the algorithm is repeated for the other RF chains.

As seen, the digital and analog parts are optimized separately in algorithm 1 and 2, respectively. The output of the Algorithm 2 that remains constant is the input of the Algorithm 1, which iteratively updates the digital part of the equalizer.

Algorithm 1 Digital Part of the Equalizer

Input: $\mathbf{W}_a$
1: $\mathbf{\Psi}^{(0)} = \mathbf{0}_U$
2: $\tilde{\mathbf{R}}_k^{(0)} = \mathbf{H}_k(\mathbf{I}_U - |\mathbf{\Psi}^{(0)}|^2)\mathbf{H}_k^H + \sigma_n^2\sigma_u^{-2}\mathbf{I}_{N_{rx}}$
3: for $i = 1, \ldots, i_{\max}$ **do**
4: $\quad \mathbf{W}_{d,k}^{(i)} = \mathbf{\Omega}_d\mathbf{H}_k^H\mathbf{W}_a\left((\mathbf{W}_a)^H\tilde{\mathbf{R}}_k^{(i-1)}\mathbf{W}_a\right)^{-1}$
5: $\quad \mathbf{B}_{d,k}^{(i)} = \left(\mathbf{W}_{d,k}^{(i)}(\mathbf{W}_a)^H\mathbf{H}_k - \mathbf{I}_U\right)\left(\mathbf{\Psi}^{(i-1)}\right)^H$
6: $\quad$ **Compute** $\mathbf{\Psi}^{(i)}$
7: $\quad \tilde{\mathbf{R}}_k^{(i)} = \mathbf{H}_k(\mathbf{I}_U - |\mathbf{\Psi}^{(i)}|^2)\mathbf{H}_k^H + \sigma_n^2\sigma_u^{-2}\mathbf{I}_{N_{rx}}$
8: end for
9: return $\mathbf{W}_{d,k}^{(i)}, \mathbf{B}_{d,k}^{(i)}$

Algorithm 2 Analog Equalizer for Dynamic Architecture

Inputs: $\mathbf{W}_{res,k,r-1}$,$\mathcal{I}$
$\mathcal{I}_r$ = Empty set, $\mathbf{w}_{a,r} = \mathbf{0}$
1: for $m = 1, \ldots, R$ do
2: $\quad \mathbf{F} = \mathbf{0}$
3: $\quad$ for $\Delta = 0, \ldots, N_\Delta - 1, p = \mathcal{A}\,\mathcal{I}$ do
4: $\quad\quad \mathbf{F}(p, \Delta) = f\left(p, R^{-1/2}e^{j2\pi\Delta/N_\Delta}\right)$
5: $\quad$ end for
6: $\quad (p_{opt}, \Delta_{opt}) = \arg \max_{p\in\mathcal{A}\ \mathcal{I}, \Delta\in\{0,\ldots,N_\Delta-1\}} \mathbf{F}(p, \Delta)$
7 $\quad \mathbf{w}_{a,r}(p_{opt}) = R^{-1/2}\exp\left(j\,2\pi\,\Delta_{opt}/N_\Delta\right)$
8: $\quad \mathcal{I}_r = [\mathcal{I}_r|p_{opt}]$
9: $\quad \mathcal{I} = [\mathcal{I}|p_{opt}]$
10: end for
11: return $\mathcal{I}$, $\mathbf{w}_{a,r}$

C. COMPLEXITY ANALYSIS

In this section, we evaluate the complexity of the proposed receiver that may be divided into two parts: 1) digital part of the equalizer computation and 2) dynamic analog equalizer part.

The computation of the digital equalizer requires the inversion of a $U \times U$ matrix and thus has complexity $O(U^3)$. Let $i_{\max}$ be the maximum number of iterations used in the digital equalizer. Then, the total complexity due to the digital part is $O(i_{\max}U^3)$.

The computation of the dynamic analog equalizer needs an evaluation of the metric in (29) for all the N_{rx} antennas and N_Δ phases. The computation of this metric requires the

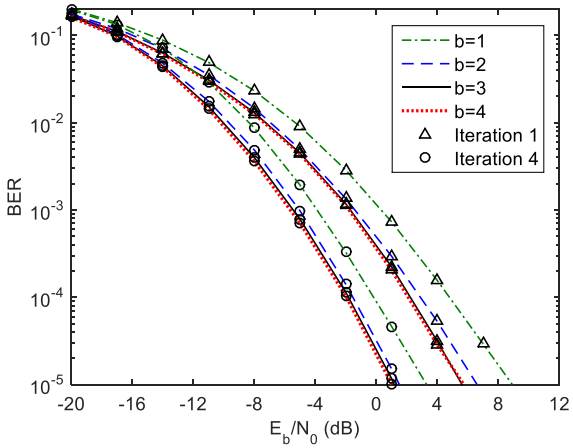

FIGURE 4. Performance of the proposed hybrid equalizer for different numbers of quantization bits, with $U = N_{rx}^{RF} = 2$, $N_{rx} = 32$, and $R = 16$.

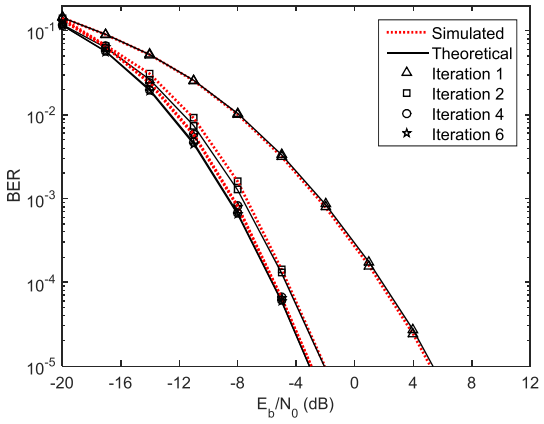

FIGURE 5. Simulated and theoretical performance of the proposed equalizer for subconnected architectures with dynamic subarray antennas, where $U = N_{rx}^{RF} = 4$ and $N_n = 64$, i.e., $R = N_{rx}/N_{rx}^{RF} = 16$.

product between a matrix and a vector for each phase and antenna, whose complexity used is $O(N_\Delta N_{rx}^2 U)$. These operations are repeated N_{rx}^{RF} times, and then the complexity of the algorithm is $O(N_{rx}^{RF} N_\Delta N_{rx}^2 U)$. Therefore the complexity of the analog part increases quadratically with the number of receive antennas. The total complexity of the proposed equalizer computation is $O(i_{\max} U^3 + N_{rx}^{RF} N_\Delta N_{rx}^2 U)$.

IV. PERFORMANCE RESULTS

The main performance results are shown in this section for the proposed hybrid receiver structure. For each UT, a wideband mmWave channel model (4) with $N_{cl} = 4$ clusters, each one with $N_{ray} = 5$ rays, is considered. As in [21], the azimuth AoD and AoA have a Laplacian distribution, and the complex path gain of the lth path from the qth cluster $\alpha_{q,l}^u$ is a random complex Gaussian variable, i.e., $\mathcal{CN}(0, 1)$. The angle spread for both the transmitters and the receiver is set to 10 degrees. We assume that the average power for all N_{cl} clusters is the same and that the path delays have a uniform distribution in the CP interval.

We assume that the antenna element spacing is half-wavelength with a carrier frequency equal to 72 GHz [39]. We also assume that the UTs and the BS employ ULAs; however, this receiver structure can be applied for other configurations. The system supports $N_c = 512$ subcarriers and a CP of length $D = N_c/4 = 128$. The length of each detected block at the BS is $S = 128$. The QPSK modulation is adopted, and a perfect synchronization and CSI are assumed at the BS side.

We present results for scenarios in which the number of transmit antennas is $N_{tx} = 16$. The results are presented in terms of BER as a function of the ratio of the average bit energy and the one-sided noise power spectral density, i.e., E_b/N_0. We assume that $E_b/N_0 = \sigma_u^2/(2\sigma_n^2) = \sigma_n^{-2}/2$ and its averages are identical for all UTs, where $\sigma_1^2 = \ldots, = \sigma_U^2 = 1$.

First, let us study the number quantization bits of phase shifters b needed to achieve the best performance. Fig. 4 shows the results for iterations 1 and 4, $U = N_{rx}^{RF} = 2$ and $N_{rx} = 32$, which means that the number of antennas per RF chain is $R = N_{rx}/N_{rx}^{RF} = 16$. From this result, we can see that increasing the number of quantized bits improves the performance as expected. It can be concluded that for the performance of $b = 3$ and $b = 4$, the curves almost overlap, and 4 quantization bits are sufficient. Hereinafter, the results are thus obtained for $b = 4$.

Now, let us evaluate the proposed hybrid multi-user equalizer for subconnected architectures with dynamic subarray antennas. First, in Fig. 5, we present the semianalytic curves for iterations 1, 2, 4, and 6, with $U = N_{rx}^{RF} = 4$ and $N_{rx} = 64$, obtained from eq. (10). The theoretical curves almost overlap with the simulation curves. Therefore, we conclude that the Gaussian approximation made in the derivation of the proposed algorithm, namely, in (31), is very accurate for all iterations and for the entire E_b/N_0 range. We also can see that the performance obtained for 4 iterations is approximately the same obtained for 6 iterations. Fig. 6 presents the BER as functions of the number of iterations for $E_b/N_0 = -5\,dB$. It can be seen that increasing the number of iterations of the digital equalizer the performance improves and the algorithm converges to a BER of $6.0 \times 10^{-5}$with a few number of iterations (4 iterations in the considered scenario). This means that 4 iterations in the digital part are enough and thus in the following figures we only present results for 1 and 4 iterations.

Then, the results are compared with the hybrid multi-user equalizer proposed in [40] for fully connected architectures and with the one in [41] for subconnected architectures with fixed subarray antennas. Fig. 7 presents the results for $U = N_{rx}^{RF} = 4$, $N_{rx} = 64$ and $R = 16$. As expected, the performance of all hybrid multi-user equalizers improves with the number of iterations. The results are only presented for 1 and 4 iterations for clarity, and for more than 4 iterations, the curves almost overlap. From Fig. 7, we can see that the proposed hybrid subconnected equalizer with dynamic antenna mapping outperforms the subconnected fixed subarray antenna equalizer for both iterations. At iteration 4, the proposed hybrid dynamic equalizer almost achieves the

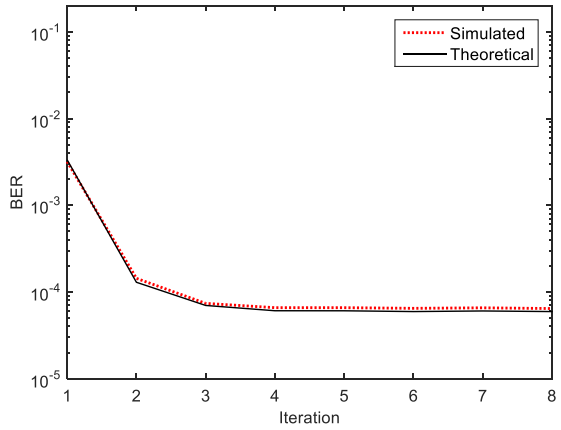

FIGURE 6. Simulated and theoretical performance for $E_b/N_0 = -5$dB of the proposed equalizer for subconnected architectures with dynamic subarray antennas, where $N_{rx} = 64$ and $N_{rx} = 64$, i.e., $R = N_{rx}/N_{rx}^{RF} = 16$.

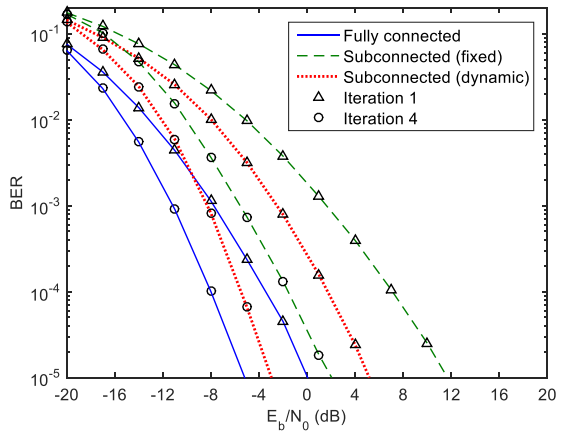

FIGURE 7. Performance comparison between the fully connected and subconnected (fixed subarray) with the proposed equalizer for subconnected architectures with dynamic subarray antennas, where $U = N_{rx}^{RF} = 4$ and $N_{rx} = 64$, i.e., $R = N_{rx}/N_{rx}^{RF} = 16$.

TABLE 2. Gap in dB between the equalizers at a target BER of 10^{-3} for the different architectures.

		Fully connected	Subconnected (dynamic)	Subconnected (fixed)
$N_{rx} = 64$	Iter. 1		6.1 dB	3.2 dB
	Iter. 4		4.2 dB	1.4 dB
$N_{rx} = 128$	Iter 1		6.0 dB	7.3 dB
	Iter. 4		3.5 dB	4.6 dB

performance of the fully connected equalizer, with lower hardware complexity. The gaps between the different equalizers at a target BER of 10^{-3} are presented in Table 2. For example, we can see in iteration 4 that there is a gain of 1.4 dB in the dynamic equalizer compared with the fixed one.

Fig. 8 presents the results for $U = N_{rx}^{RF} = 4$, $N_{rx} = 128$ and $R = 32$, where the number of receive antennas and the number of antennas per RF chain is double. As the number of RF chains is the same, only the complexity of the analog part is increased, which has a lower impact on the cost and power consumption of the overall architecture. The aim is to evaluate the performance impact of the analog part of

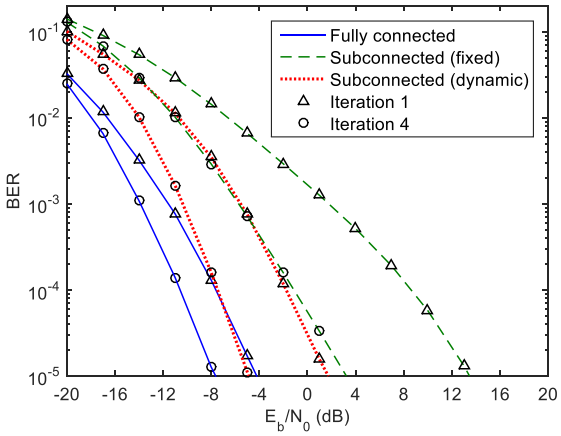

FIGURE 8. Performance comparison between the fully connected and subconnected (fixed subarray) with the proposed equalizer for subconnected architectures with dynamic subarray antennas, where $U = N_{rx}^{RF} = 4$ and $N_{rx} = 128$, i.e., $R = N_{rx}/N_{rx}^{RF} = 32$.

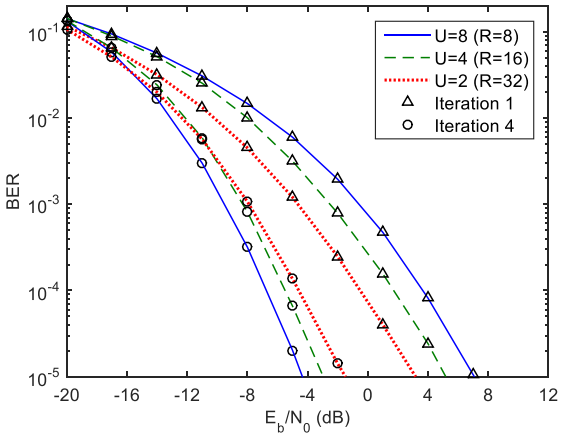

FIGURE 9. Performance comparison of the proposed equalizer for subconnected architectures with dynamic subarray antennas, where $N_{rx} = 64$.

the different equalizers while keeping the digital one approximately the same. Comparing the results of Figs. 7 and 8, we can see that the performance of the equalizers for fully connected and dynamic subconnected architectures improves when the number of receive antennas (and consequently the number of antennas per RF chain) increases. The fixed subconnected version has the worst performance because without any antenna selection criteria, the analog part deals poorly with multi-user scenarios, and the input signal in the digital part has higher levels of interference. From Table 2, we can see a gain of 4.6 dB in the dynamic equalizer compared with the fixed subconnected one. Therefore, the proposed dynamic equalizer offers a promising approach for future wireless systems where we want to reduce costs and power consumption by performing part of the processing in the analog domain.

Finally, in Fig. 9, we compare the performance of the proposed equalizer for a different number of RF chains for a fixed number of receiving antennas. The worst case (full loaded) scenario is assumed, i.e., $U = N_{rx}^{RF}$, since to separate U data streams, at least U RF chains are required. We can see from Fig. 9 that for iteration 1, the average BER performance

improves when the number of users decreases. This occurs because increasing the number of active users increases the interference level, and the digital equalizer cannot efficiently remove the interference. In contrast, for iteration 4, the average BER performance improves when the number of users increases. This occurs because as we also increase the number of RF chains at the receiver, i.e., the degrees of freedom of the digital part is also increased, and the iterative procedure of the digital part can efficiently remove the additional interference; therefore, the performance tends to the single user $1 \times N_{rx}^{RF}$ system.

V. CONCLUSIONS

In this paper, we proposed a hybrid multi-user equalizer for the uplink of broadband mmWave mMIMO SC-FDMA systems with dynamic subarray antennas. The equalizer was designed by the minimizing the sum of the MSE of all subcarriers using a two-step approach, where the digital equalizers are iterative and computed on a per subcarrier basis, while the analog equalizer, because of hardware constraints, is fixed over the iterations and subcarriers. The analog equalizer with dynamic antenna mapping was derived to connect the best set of antennas and the phase shifters to each RF chain. This was done sequentially by considering the previous antenna mapping and phase shifter values to select a new antenna and phase shifter. We also proposed a simple yet accurate semianalytical approach for obtaining the performance of the proposed scheme.

The results showed that the proposed multi-user equalizer is quite efficient at mitigating the multi-user and the inter-symbol interferences, achieving a BER performance close to the fully connected counterpart with just a few phase shifter quantization bits, thus requiring much less complexity and cost in terms of hardware. Moreover, the BER performance of the proposed equalizer outperformed the fixed subconnected counterpart. Therefore, the proposed dynamic subconnected hybrid two-step hybrid multi-user equalizer is a good choice for real broadband mmWave SC-FDMA systems employing mMIMO terminals.

APPENDIX

A. OBTAINING $\mathrm{MSE}_k^{(i)}$ EXPRESSION

For entries approximately Gaussian distributed as $\mathbf{c}_k = [c_{u,k}]_{1\le u\le U} \in \mathbb{C}^U$, it can be proven that the input-output relationship between $\mathbf{c}_k$ and $\hat{\mathbf{c}}_k^{(i)}$, $k \in \{1,\ldots,S\}$ is [38]

$$\hat{\mathbf{c}}_k^{(i)} \approx \mathbf{\Psi}^{(i)}\mathbf{c}_k + \hat{\boldsymbol{\epsilon}}_k^{(i)}, \quad k \in \{1,\ldots,S\}, \tag{31}$$

where $\hat{\boldsymbol{\epsilon}}_k^{(i)} \in \mathbb{C}^U$ is the zero mean error, uncorrelated with $\mathbf{c}_k, k \in \{1,\ldots,S\}$. The error between $\tilde{\mathbf{c}}_k^{(i)}$, given by (3), and $\mathbf{c}_k$, i.e., $\tilde{\boldsymbol{\epsilon}}_k^{(i)} = \tilde{\mathbf{c}}_k^{(i)} - \mathbf{c}_k$, is given by

$$\tilde{\boldsymbol{\epsilon}}_k^{(i)} = \underbrace{\left(\mathbf{W}_{ad,k}^{(i)}\mathbf{H}_k - \mathbf{I}_U - \mathbf{B}_{d,k}^{(i)}\mathbf{\Psi}^{(i-1)}\right)\mathbf{c}_k}_{\text{Residual ISI}} - \underbrace{\mathbf{B}_{d,k}^{(i)}\hat{\boldsymbol{\epsilon}}_k^{(i-1)}}_{\text{Errors from estimate } \hat{\mathbf{c}}_k^{(i)}} + \underbrace{\mathbf{W}_{ad,k}^{(i)}\mathbf{n}_k}_{\text{Channel Noise}}, \tag{32}$$

where we can identify three types of errors: the residual ISI, the error estimate of $\hat{\mathbf{c}}_k$, and the error due to the channel noise. From (32), we can obtain (9), making $\mathrm{MSE}_k^{(i)} = \mathbb{E}[||\tilde{\boldsymbol{\epsilon}}_k^{(i)}||^2]$ for the uth UT, using the properties of the Frobenius norm.

B. EQUIVALENCE BETWEEN $\mathrm{MSE}_k^{(i)}$ AND $\overline{\mathrm{MSE}}_k^{(i)}$

Let $\mathbf{I}_\Psi = \mathbf{I}_U - |\mathbf{\Psi}^{(i-1)}|^2$. From (9) and (12), we obtain the $\mathrm{MSE}_k^{(i)}$ as

$$\mathrm{MSE}_k^{(i)} = \left\|(\mathbf{W}_{ad,k}^{(i)}\mathbf{H}_k - \mathbf{I}_U)\mathbf{I}_\Psi^{1/2}\right\|_F^2 \sigma_u^2 + \left\|\mathbf{W}_{ad,k}^{(i)}\right\|_F^2 \sigma_n^2. \tag{33}$$

By applying the properties of the Frobenius norm to (33), we obtain

$$\begin{aligned}\mathrm{MSE}_k^{(i)} &= \mathrm{tr}\left\{(\mathbf{W}_{ad,k}^{(i)}\mathbf{H}_k - \mathbf{I}_U)\mathbf{I}_\Psi(\mathbf{W}_{ad,k}^{(i)}\mathbf{H}_k - \mathbf{I}_U)^H\sigma_u^2 \right.\\ &\quad \left. + \mathbf{W}_{ad,k}^{(i)}\left(\mathbf{W}_{ad,k}^{(i)}\right)^H\sigma_n^2\right\}\\ &= \mathrm{tr}\left\{+\mathbf{W}_{ad,k}^{(i)}\left(\sigma_u^2\mathbf{H}_k\mathbf{I}_\Psi(\mathbf{H}_k)^H + \sigma_n^2\mathbf{I}_U\right)\left(\mathbf{W}_{ad,k}^{(i)}\right)^H \right.\\ &\quad \left. - \mathbf{W}_{ad,k}^{(i)}\mathbf{H}_k\mathbf{I}_\Psi\sigma_u^2 - \mathbf{I}_\Psi(\mathbf{H}_k)^H\left(\mathbf{W}_{ad,k}^{(i)}\right)^H\sigma_u^2 + \mathbf{I}_\Psi\sigma_u^2\right\}.\end{aligned} \tag{34}$$

Replacing (14) and (15) in (34), it can be shown that the $\mathrm{MSE}_k^{(i)}$ is

$$\begin{aligned}\mathrm{MSE}_k^{(i)} = \sigma_u^2\left\|\left(\mathbf{W}_{ad,k}^{(i)} - \overline{\mathbf{W}}_{fd,k}^{(i)}\right)\left(\tilde{\mathbf{R}}_k^{(i-1)}\right)^{1/2}\right\|_F^2 \\ + \sigma_u^2\mathrm{tr}\left\{\mathbf{I}_\Psi - \overline{\mathbf{W}}_{fd,k}^{(i)}\left(\overline{\mathbf{W}}_{fd,k}^{(i)}\right)^H\right\},\end{aligned} \tag{35}$$

and by (13), definition of $\overline{\mathrm{MSE}}_k^{(i)}$, we prove that

$$\mathrm{MSE}_k^{(i)} = \sigma_u^2\overline{\mathrm{MSE}}_k^{(i)} + \sigma_u^2\mathrm{tr}\left\{\mathbf{I}_\Psi - \overline{\mathbf{W}}_{fd,k}^{(i)}\left(\overline{\mathbf{W}}_{fd,k}^{(i)}\right)^H\right\}. \tag{36}$$

C. FULL-DIGITAL EQUALIZER DERIVATION

Since the full-digital architectures are characterized by having the number of RF chains equal to the number of antennas, we can obtain the full-digital equalizer $\mathbf{W}_{fd,k}^{(i)}$, making $\mathbf{W}_a = \mathbf{I}_{N_{rx}}$ (or any other invertible square matrix, since $N_{rx}^{RF} = N_{rx}$) and then $\mathbf{W}_{fd,k}^{(i)} = \mathbf{W}_{d,k}^{(i)}[\mathbf{I}_{N_{rx}}]$. Therefore, from (17), $\mathbf{W}_{fd,k}^{(i)}$ is given by

$$\mathbf{W}_{fd,k}^{(i)} = \mathbf{\Omega}\mathbf{H}_k^H\left(\tilde{\mathbf{R}}_k^{(i-1)}\right)^{-1}, \tag{37}$$

with

$$\mathbf{\Omega} = S\left(\sum_{k=1}^{S}\mathrm{diag}\left(\mathbf{H}_k^H\left(\tilde{\mathbf{R}}_k^{(i-1)}\right)^{-1}\mathbf{H}_k\right)\right)^{-1}. \tag{38}$$

Making $\mathbf{\Omega}(\mathbf{I}_U - |\mathbf{\Psi}^{(i-1)}|^2)^{-1}\overline{\mathbf{W}}_{fd,k}^{(i)}$, we obtain (14), i.e., $\mathbf{W}_{fd,k}^{(i)} = \mathbf{\Omega}(\mathbf{I}_U - |\mathbf{\Psi}^{(i-1)}|^2)^{-1}\overline{\mathbf{W}}_{fd,k}^{(i)}$, and then $\overline{\mathbf{W}}_{fd,k}^{(i)}$ denotes a nonnormalized version of fully digital equalizer.

D. OPTIMIZATION PROBLEM (16) SOLUTION

For the optimization problem of (16), the associated Lagrangian is

$$\begin{aligned}\mathcal{L}&\left(\mu_u, \mathbf{W}_{d,k}^{(i)}\right)\\ &= \sum_{k=1}^{S}\left\|\left(\mathbf{W}_{d,k}^{(i)}\left(\mathbf{W}_{a}^{(i)}\right)^H - (\overline{\mathbf{W}}_{fd,k}^{(i)})_{opt}\right)\left(\tilde{\mathbf{R}}_k^{(i-1)}\right)^{1/2}\right\|_F^2\\ &\quad+\sum_{u=1}^{U}\mu_u \mathrm{tr}\left(\mathbf{W}_{d,k}^{(i)}\left(\mathbf{W}_{a}^{(i)}\right)^H\mathbf{H}_k\mathbf{e}_u\mathbf{e}_u^H\right)\\ &\quad\times\sum_{u=1}^{U}\mu_u\left(\sum_{k'=1,k'\neq k}^{S}\mathrm{tr}\left(\mathbf{W}_{d,k'}^{(i)}\left(\mathbf{W}_{a}^{(i)}\right)^H\mathbf{H}_{k'}\mathbf{e}_u\mathbf{e}_u^H\right)-S\right), \quad (39)\end{aligned}$$

where the coefficients μ_u, $u \in \{1, \ldots, U\}$ are the Lagrange multipliers, and $\mathbf{e}_u \in \mathbb{C}^U$. The partial derivative of (39) in order to $\mathbf{W}_{d,k}^{(i)}$ is

$$\begin{aligned}\frac{\partial\mathcal{L}\left(\mu_u, \mathbf{W}_{d,k}^{(i)}\right)}{\partial\left(\mathbf{W}_{d,k}^{(i)}\right)} &= \left(\mathbf{W}_{d,k}^{(i)}\left(\mathbf{W}_{a}^{(i)}\right)^H - \overline{\mathbf{W}}_{fd,k}^{(i)}\right)\tilde{\mathbf{R}}_k^{(i-1)}\mathbf{W}_a^{(i)}\\ &\quad+\sum_{u=1}^{U}\mu_u\mathbf{e}_u\mathbf{e}_u^H\mathbf{H}_k^H\mathbf{W}_a^{(i)}. \quad (40)\end{aligned}$$

Replacing (14) in (40), and with the result equal to zero, we have

$$\mathbf{W}_{d,k}^{(i)}\left(\mathbf{W}_{a}^{(i)}\right)^H\tilde{\mathbf{R}}_k^{(i-1)}\mathbf{W}_a^{(i)} - \mathbf{\Omega}_d\mathbf{H}_k^H\mathbf{W}_a^{(i)} = \mathbf{0}, \quad (41)$$

where $\mathbf{\Omega}_d = \mathbf{I}_U - |\mathbf{\Psi}^{(i-1)}|^2 - \sum_{u=1}^{U}\mu_u\mathbf{e}_u\mathbf{e}_u^H$ is a diagonal matrix whose entries correspond to the redefined Lagrange multipliers. The expression of the digital feedforward equalizer, (17), is then obtained from (41). From constraint $\sum_{k=1}^{S}\mathrm{diag}(\mathbf{W}_{d,k}^{(i)}(\mathbf{W}_a^{(i)})^H\mathbf{H}_k) = S\mathbf{I}_U$, we can also obtain (18).

REFERENCES

[1] Z. Pi and F. Khan, "An introduction to millimeter-wave mobile broadband systems," *IEEE Commun. Mag.*, vol. 49, no. 6, pp. 101–107, Jun. 2011.
[2] X. Gao, L. Dai, and A. M. Sayeed, "Low RF-complexity technologies to enable millimeter-wave MIMO with large antenna array for 5G wireless communications," *IEEE Commun. Mag.*, vol. 56, no. 4, pp. 211–217, Apr. 2018.
[3] C.-X. Wang, F. Haider, X. Gao, X.-H. You, Y. Yang, D. Yuan, H. M. Aggoune, H. Haas, S. Fletcher, and E. Hepsaydir, "Cellular architecture and key technologies for 5G wireless communication networks," *IEEE Commun. Mag.*, vol. 52, no. 2, pp. 122–130, Feb. 2014.
[4] Y. Xu, H. Shokri-Ghadikolaei, and C. Fischione, "Distributed association and relaying with fairness in millimeter wave networks," *IEEE Trans. Wireless Commun.*, vol. 15, no. 12, pp. 7955–7970, Dec. 2016.
[5] J.-S. Sheu, W.-H. Sheen, and T.-X. Guo, "On the design of downlink multiuser transmission for a beam-group division 5G system," *IEEE Trans. Veh. Technol.*, vol. 67, no. 8, pp. 7191–7203, Apr. 2018.
[6] C. T. Neil, A. Garcia-Rodriguez, P. J. Smith, P. A. Dmochowski, C. Masouros, and M. Shafi, "On the performance of spatially correlated large antenna arrays for millimeter-wave frequencies," *IEEE Trans. Antennas Propag.*, vol. 66, no. 1, pp. 132–148, Jan. 2017.
[7] R. Zhang, Y. Zhou, X. Lu, C. Cao, and Q. Guo, "Antenna deembedding for mmwave propagation modeling and field measurement validation at 73 GHz," *IEEE Trans. Microw. Theory Techn.*, vol. 65, no. 10, pp. 3648–3659, Oct. 2017.
[8] I. Chafaa and M. Djeddou, "Improved channel estimation in mmWave communication system," in *Proc. Seminar Detection Syst. Archit. Technol. (DAT)*, Feb. 2017, pp. 1–5.
[9] H. He, C.-K. Wen, and S. Jin, "Bayesian optimal data detector for hybrid mmWave MIMO-OFDM systems with low-resolution ADCs," *IEEE J. Sel. Topics Signal Process.*, vol. 12, no. 3, pp. 469–483, Jun. 2018.
[10] W. B. Abbas, F. Gomez-Cuba, and M. Zorzi, "Bit allocation for increased power efficiency in 5G receivers with variable-resolution ADCs," in *Proc. Inf. Theory Appl. Workshop (ITA)*, Feb. 2018, pp. 1–7.
[11] S. A. Busari, K. M. S. Huq, S. Mumtaz, L. Dai, and J. Rodriguez, "Millimeter-wave massive MIMO communication for future wireless systems: A survey," *IEEE Commun. Surveys Tuts.*, vol. 20, no. 2, pp. 836–869, 2nd Quart., 2017.
[12] P. Raviteja, Y. Hong, and E. Viterbo, "Millimeter wave analog beamforming with low resolution phase shifters for multiuser uplink," *IEEE Trans. Veh. Technol.*, vol. 67, no. 4, pp. 3205–3215, Apr. 2017.
[13] J. Zhang, L. Dai, X. Li, Y. Liu, and L. Hanzo, "On low-resolution ADCs in practical 5G millimeter-wave massive MIMO systems," *IEEE Commun. Mag.*, vol. 56, no. 7, pp. 205–211, Jul. 2018.
[14] X. Gao, L. Dai, S. Han, C.-L. I, and R. W. Heath, "Energy-efficient hybrid analog and digital precoding for MmWave MIMO systems with large antenna arrays," *IEEE J. Sel. Areas Commun.*, vol. 34, no. 4, pp. 998–1009, Apr. 2016.
[15] N. Li, Z. Wei, H. Yang, X. Zhang, and D. Yang, "Hybrid precoding for mmWave massive MIMO systems with partially connected structure," *IEEE Access*, vol. 5, pp. 15142–15151, 2017.
[16] S. Han, C.-L. I, Z. Xu, and C. Rowell, "Large-scale antenna systems with hybrid analog and digital beamforming for millimeter wave 5G," *IEEE Commun. Mag.*, vol. 53, no. 1, pp. 186–194, Jan. 2015.
[17] O. E. Ayach, S. Rajagopal, S. Abu-Surra, Z. Pi, and R. W. Heath, "Spatially sparse precoding in millimeter wave MIMO systems," *IEEE Trans. Wireless Commun.*, vol. 13, no. 3, pp. 1499–1513, Mar. 2014.
[18] W. Ni, and X. Dong, "Hybrid block diagonalization for massive multiuser MIMO systems," *IEEE Trans. Commun.*, vol. 64, no. 1, pp. 201–211, Jan. 015.
[19] R. Magueta, D. Castanheira, A. Silva, R. Dinis, and A. Gameiro, "Hybrid iterative space-time equalization for multi-user mmW massive MIMO systems," *IEEE Trans. Commun*, vol. 65, no. 2, pp. 608–620, Feb. 2017.
[20] L. Sung, D. Park, and D.-H. Cho, "Limited feedback hybrid beamforming based on dual polarized array antenna," *IEEE Commun. Lett.*, vol. 22, no. 7, pp. 1486–1489, Jul. 2018.
[21] A. Alkhateeb and R. W. Heath, "Frequency selective hybrid precoding for limited feedback millimeter wave systems," *IEEE Trans. Commun.*, vol. 64, no. 5, pp. 1801–1818, May 2016.
[22] Y.-P. Lin, "Hybrid MIMO-OFDM beamforming for wideband mmwave channels without instantaneous feedbac," *IEEE Trans. Signal Process.*, vol. 66, no. 19, pp. 5142–5151, Oct. 2018.
[23] L. Kong, S. Han, and C. Yang, "Hybrid precoding with rate and coverage constraints for wideband massive MIMO systems," *IEEE Trans. Wireless Commun.*, vol. 17, no. 7, pp. 4634–4647, Jul. 2018.
[24] R. Magueta, V. Mendes, D. Castanheira, A. Silva, R. Dinis, and A. Gameiro, "Iterative multiuser equalization for subconnected hybrid mmWave massive MIMO architecture," *Wireless Commun. Mobile Comput.*, vol. 2017, Dec. 2017, Art. no. 9171068.
[25] J. Zhang, Y. Huang, T. Yu, J. Wang, and M. Xiao, "Hybrid precoding for multi-subarray millimeter-wave communication systems," *IEEE Wireless Commun. Lett.*, vol. 7, no. 3, pp. 440–443, Jun. 2017.
[26] J. Du, W. Xu, H. Shen, X. Dong, and C. Zhao, "Hybrid precoding architecture for massive multiuser MIMO with dissipation: Sub-connected or fully connected structures?" *IEEE Trans. Wireless Commun.*, vol. 17, no. 8, pp. 5465–5479, Aug. 2018.
[27] F. Sohrabi and W. Yu, "Hybrid analog and digital beamforming for mmWave OFDM large-scale antenna arrays," *IEEE J. Sel. Areas Commun.*, vol. 35, no. 7, pp. 1432–1443, Jul. 2017.
[28] L. He, J. Wang, and J. Song, "Generalized spatial modulation aided mmWave MIMO with sub-connected hybrid precoding scheme," in *Proc. IEEE Global Commun. Conference (GLOBECOM)*, Dec. 2017, pp. 1–6.
[29] Y. Huang, J. Zhang, and M. Xiao, "Constant envelope hybrid precoding for directional millimeter-wave communications," *IEEE J. Sel. Areas Commun.*, vol. 36, no. 4, pp. 845–859, Apr. 2018.
[30] S. Park, A. Alkhateeb, R. W. Heath , "Dynamic subarrays for hybrid precoding in wideband mmWave MIMO systems," *IEEE Trans. Wireless Commun.*, vol. 16, no. 5, pp. 2907–2920, May 2017.

[31] D. Zhang, Y. Wang, X. Li, and W. Xiang, "Hybridly connected structure for hybrid beamforming in mmWave massive MIMO systems," *IEEE Trans. Commun.*, vol. 66, no. 2, pp. 662–674, Feb. 2018.
[32] F. Pancaldi, and G. M. Vitetta , "Frequency-domain equalization for space-time block-coded systems," *IEEE Trans. Wireless Commun.*, vol. 4, no. 6, pp. 2907–2916, Nov. 2005.
[33] R. Dinis, R. Kalbasi, D. Falconer, and A. H. Banihashemi, "Iterative layered space-time receivers for single-carrier transmission over severe time-dispersive channel," *IEEE Commun. Lett.*, vol. 8, no. 9, pp. 579–581, Sep. 2004.
[34] J. Silva, R. Dinis, N. Souto, and P. Montezuma, "Single-carrier frequency domain equalisation with hierarchical constellations: An efficient transmission technique for broadcast and multicast systems," *IET Commun.*, vol. 6, no. 13, pp. 2065–2073, Sep. 2012.
[35] A. Silva, S. Teodoro, R. Dinis, and A. Gameiro, "Iterative frequency-domain detection for IA-precoded MC-CDMA systems," *IEEE Trans. Commun.*, vol. 62, no. 4, pp. 1240–1248, Apr. 2014.
[36] A. Silva, J. Assunção, R. Dinis, and A. Gameiro, "Performance evaluation of IB-DFE-based strategies for SC-FDMA systems," *EURASIP J. Wireless Commun. Netw.*, vol. 2013, no. 1, pp. 1–10, Dec. 2013.
[37] D. Castanheira, A. Silva, R. Dinis, and A. Gameiro, "Efficient transmitter and receiver designs for SC-FDMA based heterogeneous networks," *IEEE Trans. Commun.*, vol. 63, no. 7, pp. 2500–2510, Jul. 2015.
[38] H. E. Rowe, "Memoryless nonlinearities with Gaussian inputs: Elementary results," *Bell Syst. Tech. J.*, vol. 61, no. 7, pp. 1519–1525, Sep. 1982.
[39] T. S. Rappaport, G. R. MacCartney, M. K. Samimi, and S. Sun, "Wideband millimeter-wave propagation measurements and channel models for future wireless communication system design," *IEEE Trans. Commun.*, vol. 63, no. 9, pp. 3029–3056, Sep. 2015.
[40] R. Magueta, D. Castanheira, A. Silva, R. Dinis, and A. Gameiro, "Two-step analog-digital multiuser equalizer for hybrid precoded mmWave communications," in *Proc. IEEE Global Commun. Conf. (GLOBECOM)*, Dec. 2018, pp. 1–6.
[41] R. Magueta, D. Castanheira, A. Silva, R. Dinis, and A. Gameiro, "Two-step hybrid multiuser equalizer for sub-connected mmWave massive MIMO SC-FDMA systems," in *Proc. Eur. Signal Process. Conf. (EUSIPCO)*, Sep. 2018, pp. 1–5.

ROBERTO MAGUETA received the M.Sc. degree in electronics and telecommunications engineering from the University of Aveiro, Portugal, in 2013. He is currently pursuing the Ph.D. degree. He joined the Instituto de Telecomunicações, Aveiro, as a Researcher with the Project RadioVoip-Smart Antenna for Maritime Communications. He has been involved in some national and European projects, namely PURE-5GNET, and HETCOP, within the FCT Portuguese National Scientific Foundation. His thesis' work is focused on transmitter and receiver designs for future mm-wave and massive MIMO-based wireless systems. His research interests include antenna design, multicarrier based systems, precoding and multiuser detection, massive MIMO, and millimeter wave communications.

DANIEL CASTANHEIRA received the Licenciatura (ISCED level 5) and Ph.D. degrees in electronics and telecommunications from the University of Aveiro, in 2007 and 2012, respectively. He is currently an Auxiliary Researcher with Instituto de Telecomunicações, Aveiro, Portugal. He has been involved in several national and European projects, namely RETIOT, SWING2, PURE-5GNET, HETCOP, COPWIN, PHOTON, within the FCT Portuguese National Scientific Foundation, and CODIV, FUTON and QOSMOS with the FP7 ICT. In 2011, he was with the "Departamento de Eletrónica, Telecomunicações e Informática," Aveiro University, as an Assistant Professor. His research interests include signal processing techniques for digital communications, with emphasis for physical layer issues including channel coding, precoding/equalization, and interference cancelation.

ADÁO SILVA received the M.Sc. and Ph.D. degrees in electronics and telecommunications from the University of Aveiro, in 2002 and 2007, respectively. He is currently an Assistant Professor with the Department of Electronics, Telecommunications and Informatics of the University of Aveiro, and Senior Researcher with the Instituto de Telecomunicações. He has been participating in several national and European projects, namely the ASILUM, MATRICE, 4MORE, within the ICT programme and the FUTON and CODIV projects with the FP7 ICT. He has led several research projects, in the broadband wireless communications area, at the national level. He acted as a member of the TPC of several international conferences. His research interests include multiuser MIMO, multicarrier based systems, cooperative networks, precoding, multiuser detection, massive MIMO, and millimeter wave communications.

RUI DINIS received the Ph.D. degree from Instituto Superior Técnico (IST), Technical University of Lisbon, Portugal, in 2001, and the Habilitation in telecommunications from the Faculdade de Ciências e Tecnologia (FCT), Universidade Nova de Lisboa (UNL), in 2010. From 2001 to 2008, he was a Professor with IST. He is currently an Associate Professor with FCT–UNL. In 2003, he was an Invited Professor with Carleton University, Ottawa, Canada. He was a Researcher with CAPS (Centro de Análise e Processamento de Sinal), IST, from 1992 to 2005, and a Researcher with ISR (Instituto de Sistemas e Robótica) from 2005 to 2008. Since 2009, he has been a Researcher with IT (Instituto de Telecomunicações). He is an Editor of the IEEE TRANSACTIONS ON COMMUNICATIONS (Transmission Systems - Frequency-Domain Processing and Equalization) and the IEEE TRANSACTIONS ON VEHICULAR TECHNOLOGY. He was also a Guest Editor for Elsevier Physical Communication (Special Issue on Broadband Single-Carrier Transmission Techniques). He has been actively involved in several national and international research projects in the broadband wireless communications area. His research interests include modulation, equalization, channel estimation, and synchronization.

ATÍLIO GAMEIRO received the Licenciatura and Ph.D. degrees from the University of Aveiro, in 1985 and 1993, respectively. He is currently an Associate Professor with the Department of Electronics and Telecommunications of the University of Aveiro, and a Researcher with the Instituto de Telecomunicações, Pólo de Aveiro, where he is the head of the group. His industrial experience includes a period of one year with BT Labs and one year with NKT Elektronik. His current research-interests include signal processing techniques for digital communications and communication protocols, and within this research line he has done work for optical and mobile communications, either at the theoretical and experimental level. He has published over 200 technical papers in international journals and conferences. His current research activities involve space-time-frequency algorithms for the broadband wireless systems and cross-layer design. He has been involved and has led IT or University of Aveiro participation on more than 20 national and European projects.